Inorganica Chimica Acta 433 (2015) 3–12

Contents lists available at ScienceDirect

Inorganica Chimica Acta

journal homepage: www.elsevier.com/locate/ica

Carbonyl group coordination preferences in square-planar Ni^{II} and Pd^{II} complexes of pentadentate ligands by electron-withdrawing/donating substituents

Jianlin Han [a], José Luis Aceña [b], Nobuhiro Yasuda [c], Hidehiro Uekusa [d], Taizo Ono [e], Vadim A. Soloshonok [b,f,*], Karel D. Klika [g,h,*]

[a] School of Chemistry and Chemical Engineering, Nanjing University, Nanjing 210093, China
[b] Department of Organic Chemistry I, Faculty of Chemistry, University of the Basque Country UPV/EHU, Paseo Manuel Lardizábal 3, 20018 San Sebastián, Spain
[c] Japan Synchrotron Radiation Research Institute, SPring-8, 1-1-1 Kouto, Sayo-gun, 679-5198 Sayo-cho, Hyogo, Japan
[d] Department of Chemistry and Materials Science, Tokyo Institute of Technology, Ookayama 2, Meguro-ku, Tokyo 152-8551, Japan
[e] National Institute of Advanced Industrial Science and Technology (AIST), Anagahora 2266-98, Shimoshidami, Moriyama, 463-8560 Nagoya, Aichi, Japan
[f] IKERBASQUE, Basque Foundation for Science, María Díaz de Haro 3, 48013 Bilbao, Spain
[g] Department of Chemistry, University of Turku, Vatselankatu 2, FIN-20014 Turku, Finland
[h] Molecular Structure Analysis, German Cancer Research Center (DKFZ), Im Neuenheimer Feld 280, D-69009 Heidelberg, Germany

ARTICLE INFO

Article history:
Received 26 February 2015
Received in revised form 20 April 2015
Accepted 27 April 2015
Available online 7 May 2015

Keywords:
Ni^{II} complexes
Pd^{II} complexes
Trifluoromethyl group
Chiral switches
Coordination modes
Density functional theory

ABSTRACT

A series of chirally switchable Ni^{II} and Pd^{II} complexes were synthesized and fully characterized by X-ray crystallography and additionally by NMR. It was found that control of the stereochemical preference between (S^*,S^*) and (S^*,R^*) diastereomers by substituent modification of the ligand sidearms was possible in the process of crystallization with the preferred coordination of the sidearms generally consistent with expectations based on the electron-donating or -withdrawing properties of the sidearm substituent groups. There were however, quite interesting and unanticipated exceptions counter to chemical intuition and it seems that only for complexes with *ortho* substituents are strong preferences for the coordination manner necessarily displayed in the solid state based on the electron-withdrawing or -donating properties of the substituents.

1. Introduction

Molecules that can form supramolecular assemblies frequently possess useful chemical and physical properties [1], and amongst these coordination compounds are particularly prominent since one of the major challenges is to attain a fine balance between structural predictability and coordination flexibility, thereby allowing the compounds to be responsive to external stimuli [2]. In this respect, one successful approach has been the application of ligands containing carbonyl groups specifically intended to be weakly coordinating [3]. We previously introduced a molecular system based on the coordination of achiral pentadentate ligands with d^8 metals [4], and have since extended it to chiral ligands [5]. Such chirally facile interconverting systems have been adopted recently for their potential application as molecular switches [6], though the authors drew attention to the inherent drawback in that no chemical reaction can proceed with 100% conversion [4a]. This is countered however, by the plethora of potential systems that could be applied for such purposes [6].

In our system consisting of square-planar Ni^{II} or Pd^{II} complexes (Scheme 1), two elements of chirality are present: the stereogenic center resulting from the fixation of the chirality at the benzylamine nitrogen and the stereogenic axis arising from the restricted rotation of the non-coordinated *N*-(*o*-benzophenone) amide moiety about the N–C bond. Four species altogether, discounting enantiomers, are possible when utilizing differently substituted sidearms of the ligand and facile interconversion could conceivably occur between two preferred species. For example, the switch between diastereomers (S^*,S^*) and (S^*,R^*) occurs via the carbonyl de-coordination/coordination step resulting in

* Corresponding authors at: Department of Organic Chemistry I, Faculty of Chemistry, University of the Basque Country UPV/EHU, Paseo Manuel Lardizábal 3, 20018 San Sebastián, Spain. Tel.: +34 943 015177; fax: +34 943 015270 (V.A. Soloshonok). Molecular Structure Analysis, German Cancer Research Center (DKFZ), Im Neuenheimer Feld 280, D-69009 Heidelberg, Germany. Tel.: +49 6221 42 4515; fax: +49 6221 42 2995 (K.D. Klika).

E-mail addresses: vadym.soloshonok@ehu.es (V.A. Soloshonok), klikakd@yahoo.co.uk (K.D. Klika).

http://dx.doi.org/10.1016/j.ica.2015.04.029
0020-1693/

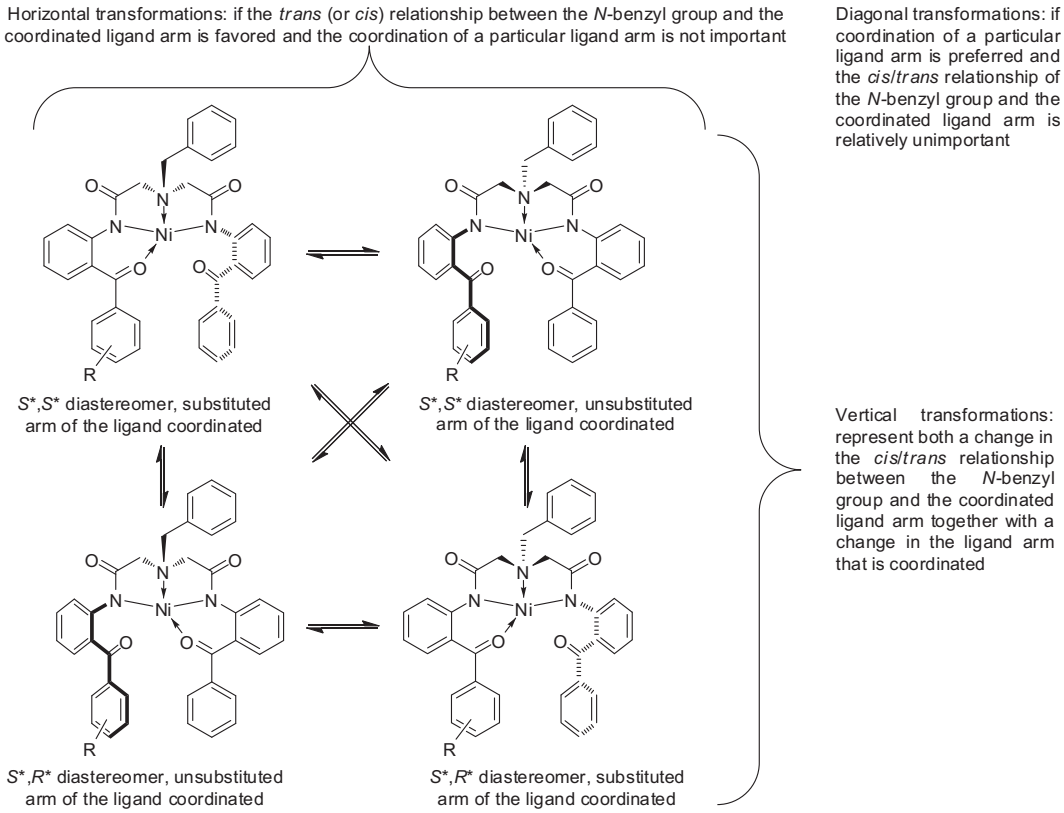

Scheme 1. Formation of diastereomerically switchable complexes from chiral ligands.

inversion of the stereogenic center chirality whilst retaining the same sense of the axial chirality, i.e. the vertical transitions in Scheme 1.[1] If retention of the *cis*/*trans* relationship of the *N*-benzyl group and the coordinated ligand arm is favored but the coordinating sidearm is not, then the horizontal transformations are in operation while conversely if the *cis*/*trans* relationship of the *N*-benzyl group and the coordinated ligand arm is unimportant but the coordinating sidearm is, then the diagonal transformations are in effect. Importantly, it should be noted that due to the structural rigidity of the complexes, a process such as the vertical transition can occur with near complete (>99%) stereoselectivity.

Previously, to evolve the molecular system with differently substituted sidearms in terms of predictability, we introduced electron-withdrawing or -donating substituents to influence the preference for coordination of the *N*-(*o*-benzophenone) amide carbonyls [5]. While the reported data were quite convincing, we felt that only two examples for the Ni^{II} and one for the Pd^{II} complexes were insufficient to consider this approach for controlling the coordination preferences completely explored and proven. Therefore, we decided to extend our study to the synthesis of an additional series of fluorinated and non-fluorinated Ni^{II} and Pd^{II} complexes to further understand the processes and factors involved in the system interconversion, the preferential binding modes, as well as peculiarities of the crystallographic packing. Characterization of the complexes was enabled in the solid state by X-ray crystallographic analysis supported by NMR and MS measurements. The relative energies of the structures with respect to configuration and coordination site were evaluated by DFT calculations to further complement and comprehend the results.

[1] The assignment of configuration at the stereogenic center, the N atom, follows the convention outlined previously (Ref. [5]) in that covalent bonds are not considered to take undue preference over coordinating bonds.

2. Results and discussion

Continuing our modular approach for the design and synthesis of pentadentate ligands and the consequent metal complexes [7], we prepared ligands **5a**–**c** in high yields, starting from the acetyl-protected 2-aminobenzophenones **1a**–**c**, readily available by aryl Grignard additions to 2-methyl-4*H*-3,1-benzoxazin-4-one (Scheme 2). **1a**–**c** were first hydrolyzed to the free 2-aminobenzophenones **2a**–**c**, and then converted to amides **3a**–**c** by treatment with bromoacetyl bromide. These compounds encompassed electron-donating *ortho*-methyl, –*o*-Me, (**3a**) and *para*-methoxy, –*p*-OMe, (**3c**) groups as well as an electron-withdrawing *para*-trifluoromethyl, –*p*-CF_3, (**3b**) group. Compounds **3a**–**c** were transformed to pentadentate ligands **5a**–**c** by reaction with the ring-unsubstituted benzlyamine moiety **4** [7c], also in high yields. Treatment of **3c** (Scheme 3) with benzylamine yielded intermediate **7** [5,8], which upon reaction with **3b** yielded pentadentate ligand **8** functionalized on both sidearms, again in high yield.

The synthesis of Ni^{II} and Pd^{II} complexes **6a**–**e** (Schemes 2 and 3) proceeded straightforwardly by the reaction of $Ni(NO_3)_2{\cdot}6H_2O$ (**6b**,**d**,**e**) or $PdCl_2$ (**6a**,**c**) together with the appropriate ligand (**5a**–**c** or **8**) in methanol under basic conditions [7c,9], though with only modest (Ni complexes) or poor (Pd complexes) yields being obtained.

Crystals of complexes **6a**–**e** amenable for X-ray analysis were obtained in each case by slow evaporation from either CH_2Cl_2 (**6b**–**e**) or EtOAc (**6a**) solutions overlaid with *n*-hexane. This usually required great perseverance and was very demanding and only very small crystals could be obtained in some cases. The details of X-ray crystallographic data collection and refinement for Ni^{II} and Pd^{II} complexes **6a**–**e** are summarized in Table 1.

Previously we have examined CF_3-containing Ni^{II} and Pd^{II} complexes **6f**–**h** (Fig. 1) and found full consistency between the

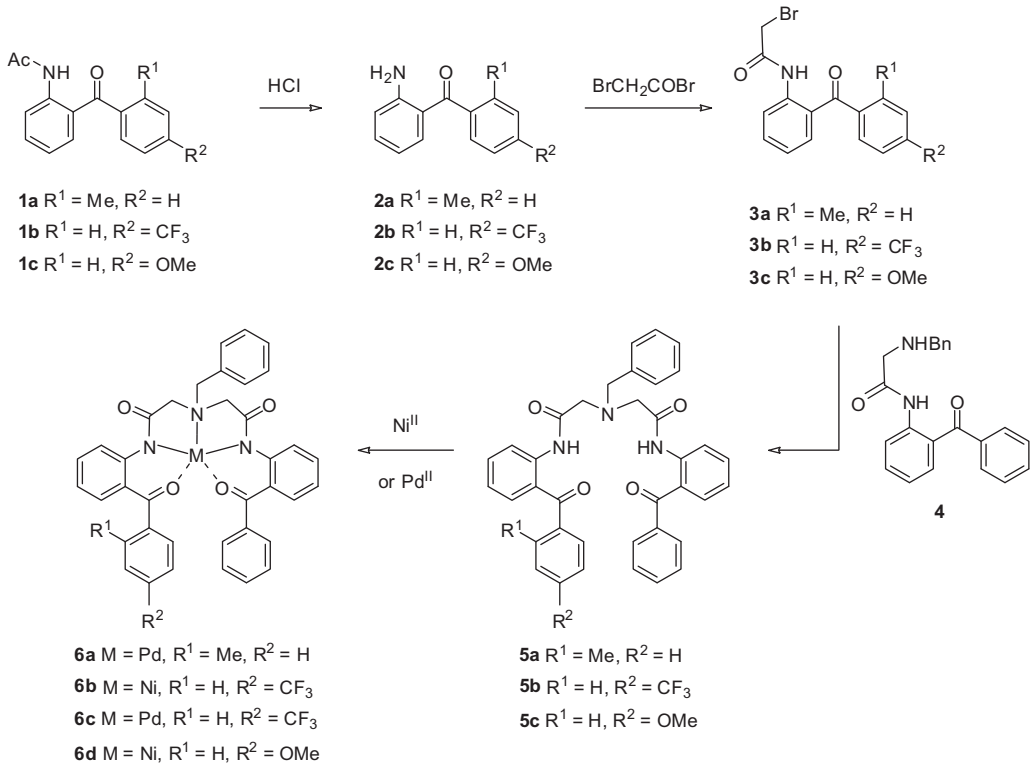

Scheme 2. Synthesis of ligands **5a–c** and Ni^{II} and Pd^{II} complexes **6a–d**. N.b. The actual coordinating sidearm is described in turn for each complex **6a–d**.

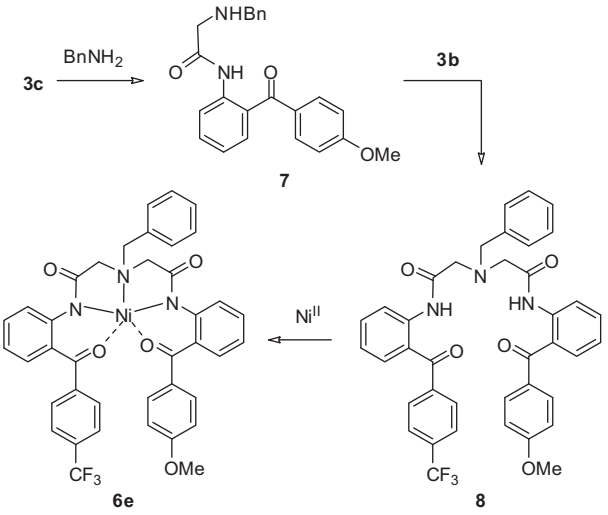

Scheme 3. Synthesis of Ni^{II} complex **6e**.

anticipated and the observed coordination in the solid state as determined by X-ray crystallographic analysis [5]. The anticipated coordination preference was considered in light of the electron-donating or -withdrawing properties of the sidearm substituent groups and can be construed as "chemical intuition".

All five Ni^{II} complexes **6b**,**d–g** from these two studies were found to crystallize in the triclinic system and space group $P\bar{1}$ with two molecules per unit cell consisting of an enantiomeric pair of molecules, *R*,*R* and *S*,*S*. All three Pd^{II} complexes **6a**,**c**,**h** on the other hand, were found to crystallize in the orthorhombic system, though formerly **6h** was found to crystallize in the space group *Pbca* while in this study **6a**,**c** both were found to crystallize in the space group *Pccn*. All three Pd^{II} crystal structures however, contained eight molecules per unit cell consisting of four enantiomeric pairs of molecules, *R*,*R* and *S*,*S*.

The Ni^{II} complex **6b** exhibited the expected coordination manner in the solid state (Fig. 2) in that the carbonyl oxygen of the unsubstituted sidearm of the ligand was preferentially coordinated to the Ni due to the electron-withdrawing property of the –*p*-CF_3 substituent group in the non-coordinated arm thus favoring preferential coordination by the carbonyl oxygen to the Ni in the former sidearm. This same observation held true for Pd^{II} complex **6c** in the solid state (Fig. 3) via similar reasoning. Thus, re-positioning the –CF_3 group from the *ortho* position, i.e. Ni^{II} complex **6f** where the resonance effects might be expected to be stronger in addition to sigma effects, still results in the same preferred coordination manner in the solid state.

In the previous study, we examined the tandem effect of mixing electron-donating (–*p*-OMe) and -withdrawing (–*o*-CF_3) substituent groups with one of each type on opposing arms [5]. Unsurprisingly, both the Ni^{II} (**6g**) and Pd^{II} complexes (**6h**) exhibited the expected manner of coordination preference in the solid state with the carbonyl oxygen of the sidearm containing the –*p*-OMe substituent group being coordinated to the metal.

We again examined the tandem effect of mixing electron-donating and -withdrawing substituent groups with one of each type on opposing arms, but this time with –*p*-OMe and –*p*-CF_3 substituent groups, i.e. the –CF_3 group was re-positioned from the *ortho* position to the *para* position in Ni^{II} complex **6e** with respect to complexes **6g**,**h**. The ensuing result was remarkable. The molecular structure of **6e** displayed structural disorder at the two terminal functional groups, –*p*-CF_3 and –*p*-OMe, in which the positions of –*p*-CF_3 and –*p*-OMe are exchanged (i.e. the coordinating sidearms are interchanged). These disordered –*p*-CF_3 and –*p*-OMe groups are almost completely overlapped at the two sites as they have very similar geometric volumes, so such disorder can thus occur without steric hindrance in the crystal structure and disruption of the crystal packing forces. Though this is a known

Table 1
Summary of crystal data for complexes **6a–e**.

	6a	6b	6c	6d	6e
Formula	$C_{38}H_{31}N_3O_4Pd$	$C_{39}H_{30}Cl_2F_3N_3O_4Ni$	$C_{38}H_{28}F_3N_3O_4Pd$	$C_{39}H_{33}Cl_2N_3O_5Ni$	$C_{40}H_{32}Cl_2F_3N_3O_5Ni$
M	700.06	791.27	754.03	753.27	821.30
Temperature (K)	123(2)	143(2)	123(2)	123(2)	123(2)
Wavelength (Å)	0.68972	1.54186	0.83136	0.83136	0.71073
Crystal size (mm)	0.0879 × 0.0159 × 0.005	0.07 × 0.02 × 0.02	0.0876 × 0.0164 × 0.005	0.170 × 0.0143 × 0.0043	0.40 × 0.06 × 0.04
Crystal system	orthorhombic	triclinic	orthorhombic	triclinic	triclinic
Space group	*Pccn*	$P\bar{1}$	*Pccn*	$P\bar{1}$	$P\bar{1}$
a (Å)	23.474(3)	8.5200(2)	23.5859(9)	8.5849(4)	8.6277(7)
b (Å)	31.104(5)	13.6980(3)	31.8655(10)	13.7098(8)	14.1581(12)
c (Å)	8.5425(15)	15.8800(4)	8.3357(3)	15.4024(9)	15.9486(13)
α (°)	–	75.748(1)	–	78.1456(19)	71.537(2)
β (°)	–	75.510(1)	–	73.6561(17)	78.720(2)
γ (°)	–	83.215(1)	–	82.8312(16)	86.163(2)
V (Å^3)	6237.3(17)	1735.97(7)	6265.0(4)	1698.13(16)	1812.2(3)
Z	8	2	8	2	2
D_{calc} (Mg m^{-3})	1.491	1.514	1.599	1.473	1.505
F(000)	2869	812	3056	780	844
θ Range for data collection (°)	1.68–24.55	2.95–68.23	2.46–27.89	2.63–27.83	3.03–27.45
Index ranges, *hkl*	−27 to 28, −37 to 37, −10 to 10	−10 to 9, −16 to 16, −18 to 19	−19 to 26, −30 to 30, −8 to 9	−8 to 7, −15 to 15, −17 to 17	−11 to 11, −18 to 18, −20 to 20
Reflections unique/observation	5705/38442	6237/20534	3664/21851	4249/8751	8045/17496
Goodness-of-fit on F^2	0.248	1.000	1.055	1.084	1.070
Final *R* indices {$I > 2\sigma(I)$}, R_1, wR_2	0.0298, 0.0422	0.1641, 0.3545	0.0514, 0.1089	0.0978, 0.2350	0.0608, 0.1418
R indices (all data), R_1, wR_2	0.1710, 0.0598	0.4261, 0.5224	0.0870, 0.1244	0.1435, 0.2881	0.1087, 0.1757
Largest diff. peak, hole (e Å^{-3})	0.379 and −0.443	0.713 and −0.607	0.681 and −1.162	1.179 and −0.961	1.293 and −0.964

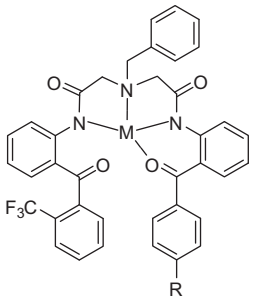

6f M = Ni, R = H
6g M = Ni, R = OMe
6h M = Pd, R = OMe

Fig. 1. The previously reported Ni^{II} and Pd^{II} complexes **6f–h** [5].

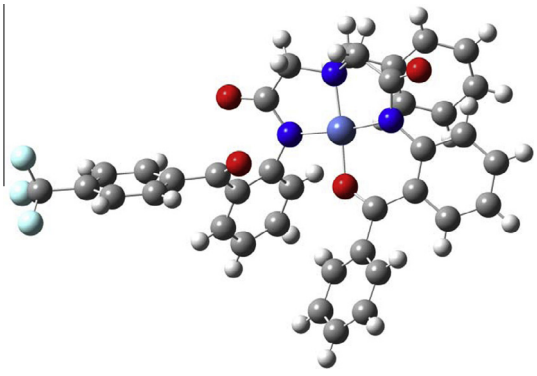

Fig. 2. X-ray structure of Ni^{II} complex **6b**; only the (*S*,*S*)-enantiomer is shown from the unit cell containing both enantiomers.

phenomenon – the isomorphic or "chloro–methyl" exchange rule [10] – the occupancy factor of the minor component (the carbonyl oxygen of the sidearm bearing the –*p*-CF_3 group being coordinated to the Ni) however, is only 0.103(5) and this is somewhat unusual. The occupancy anomaly may originate from crystallographic sources [10], e.g. insufficient void space around the two groups resulting in less than rigid but not totally slack packing or insufficient molecular size to completely negate the differences in surface charge between the two groups. Alternatively, minor stability differences in the adopted coordinations could result in both species being present to a high degree in solution. Clearly the latter must be an important factor in this case and therefore the conclusion must be that the effect of the electron-donating properties of the –*p*-OMe substituent group and the electron-withdrawing properties of the –*p*-CF_3 substituent group can be considered quite weak despite the contrary indications for the latter from complexes **6b**,**c** (vide supra). The structure of Ni^{II} complex **6e** with an indication of the disorder at the substituent sites is displayed in Fig. 4.

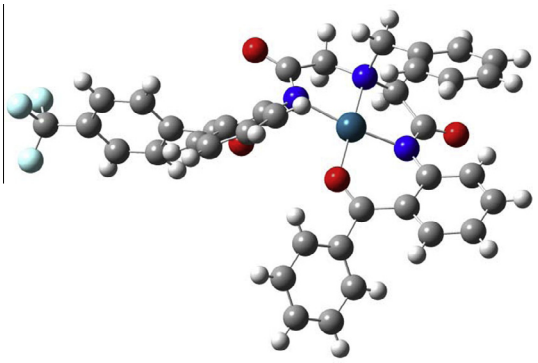

Fig. 3. X-ray structure of Pd^{II} complex **6c**; only the (*R*,*R*)-enantiomer is shown from the unit cell containing both enantiomers.

The Pd^{II} complex **6a** with an –*o*-Me substituent group exhibited the expected coordination manner in the solid state (Fig. 5) in that the carbonyl oxygen of the substituted sidearm of the ligand was preferentially coordinated to the Pd due to the electron-donating property of the –*o*-Me substituent group in the coordinating arm thus favoring preferential coordination by its carbonyl oxygen to the Pd.

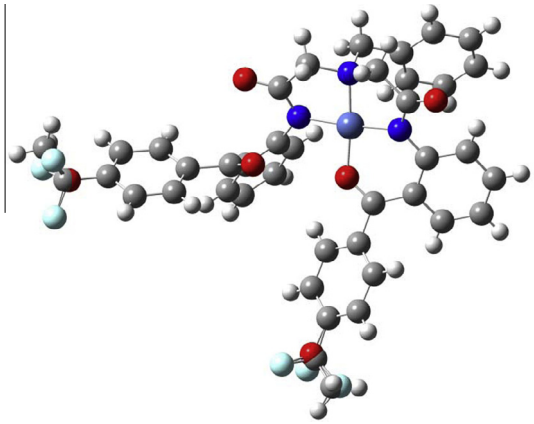

Fig. 4. X-ray structure of Ni^{II} complex **6e**; only the (*S*,*S*)-enantiomer is shown from the unit cell containing both enantiomers. The disorder at the –p-OMe and –p-CF3 substituent groups is portrayed.

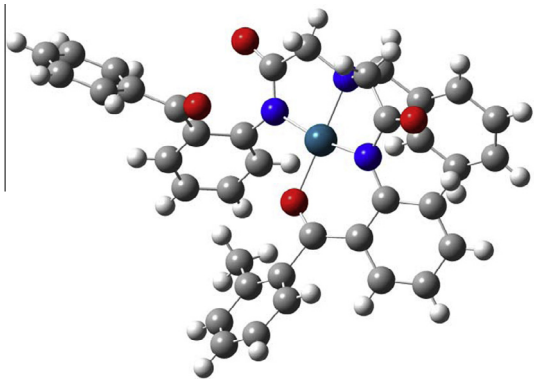

Fig. 5. X-ray structure of Pd^{II} complex **6a**; only the (*S*,*S*)-enantiomer is shown from the unit cell containing both enantiomers.

Finally, the solid state structure of Ni^{II} complex **6d** with an electron-donating –*p*-OMe substituent group – previously indicated to be only weakly effective from the results of **6e** – is presented in Fig. 6. The result is, in spite the aforementioned assertion, still unexpected and quite extraordinary. The carbonyl oxygen in the unsubstituted sidearm is preferentially coordinated to the Ni counter to chemical intuition. It can only be assumed that crystal packing forces may play a determinate role in exhibiting the unexpected coordination manner in the solid state. To rationalize this intriguing result, it is worth noting that complexes **6b**–**d** are all isostructural and it is the carbonyl oxygen of the unsubstituted sidearm that is coordinated to the metal: It seems therefore that only for complexes with *ortho* substituents (complexes **6a**,**f**–**g**) are strong preferences necessarily displayed in the solid state based on the electron-withdrawing or -donating properties of the substituents. In other cases with only *para* substituents present (complexes **6b**–**e**), the observed preference for the coordination manner may align with the expected preference, though this may simply be incidental (complexes **6b**,**c**), or it may provide an unexpected mixture (complex **6e**), or it may provide a seemingly anomalous result counter to chemical intuition (complex **6d**). As a final note, the *cis* isomers were not observed at all, and thus only the (*S*,*S*)- and (*R*,*R*)-enantiomers were present representing the *trans* isomers.

To try and comprehend these anomalous solid-state results, recourse was made to NMR measurements and DFT calculations.

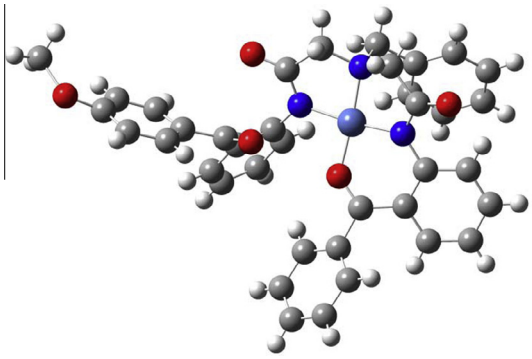

Fig. 6. X-ray structure of Ni^{II} complex **6d**; only the (*S*,*S*)-enantiomer is shown from the unit cell containing both enantiomers.

The complexes **6a**–**h**, unfortunately, were only very poorly soluble in suitable solvents, thus limiting their comprehensive analysis by NMR, limited especially by the consequent unavailability of ^{13}C acquisition. With appreciable conformational mobility including the flexible benzyl moiety, fluxional motion of the heteroatom rings formed by coordination to the metal, and other bond rotations etc., in addition to the chiral switching arising from the decoordination/coordination steps of the carbonyl oxygen atoms to the metal, the NMR spectra were either extremely broad or contained multiple resonances from the various contributing species wherein interconversion between the species was confirmed by variable-temperature NMR. Thus pertinently, the solution-state flexibility extends to the solid state as discussed above.

Nevertheless, the evaluation of Gibbs' Free Energies (ΔG) for the equilibria based on signal integration to access populations enabled comparison to ΔG values provided by DFT-calculations and is discussed in conjunction with the modeling results (vide infra). For characterization purposes of these complexes, sufficient ^{1}H and ^{19}F NMR data were nonetheless attained and were consistent with the expected structures. Irrespective of these limitations however, the dynamic behaviors exhibited by the complexes clearly indicate the potential for facile switching between diastereomers and clearly chiral switching must be a principle process in effect based on the magnitude of the energies involved. Moreover, it was evident that the introduction of electron-withdrawing or -donating substituents on the sidearms in ligands **5a**–**c** and **8** was insufficient for providing a predictable, overwhelmingly biased coordination of a particular carbonyl group in solution. An interesting point however, is that the δ_F of the coalesced signal for the $-CF_3$ group for complexes **6b**,**c**,**e** is essentially identical in all three cases (ca. -65 ± 1 ppm), thus pertaining to at least some dominance of the species where the carbonyl oxygen in the ligand arm bearing the $-CF_3$ group is not coordinated to the metal, otherwise it could be expected that differences in δ_Fs would be apparent – notwithstanding some quite improbable coincidences in δ_F and equilibria positions. This is analogous to complexes **6f**–**h** which also displayed [5] an essentially identical δ_F of the coalesced signal for their $-CF_3$ group (ca. -61 ppm) with the difference in δ_F between the two sets attributed to the *ortho*/*para* positioning of the $-CF_3$ substituent group.

For comparison to the experimental NMR results, four coordination site/relative configuration permutations were selected for intrastructural evaluation of each complex and interstructural comparison between the complexes following geometry optimization and calculation of their corresponding energies by density functional theory (DFT) quantum chemical calculations. The four structural permutations of each complex were the coordination of either carbonyl of each ligand arm to the metal and then with

respect to the relative configuration of the free ligand arm as either *cis* (i.e. R^*,S^*) or *trans* (i.e. R^*,R^*) to the benzyl group. Each structure for optimization was conveniently modified from an optimized structure taken from a set for a compound previously optimized. This ensured firstly, computational efficiency, and secondly, fair comparison between the analogous structures across the sets. Calculations were performed firstly in the gas phase, and then by inclusion of a solvent model (polarizable continuum model using the integral equation formalism variant, IEFPCM) for CH_2Cl_2. The non-metallic atoms were adequately handled using the restricted B3LYP functional with the 6-31G(d,p) basis set while the Ni and Pd entities necessitated the selective use of the LanL2DZ basis set. Example depictions for Ni^{II} complex **6b** of the four structural permutations are presented in Figs. 7–10 while Table 2 lists the

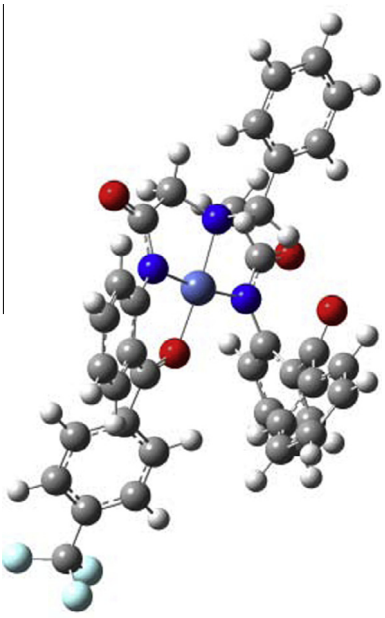

Fig. 7. Complex **6b** with coordination of the ligand arm bearing the $-CF_3$ group and with the unsubstituted ligand arm *cis* to the benzyl group.

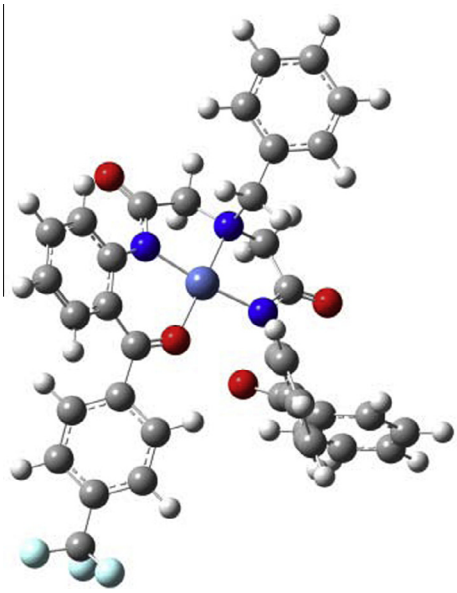

Fig. 8. Complex **6b** with coordination of the ligand arm bearing the $-CF_3$ group and with the unsubstituted ligand arm *trans* to the benzyl group.

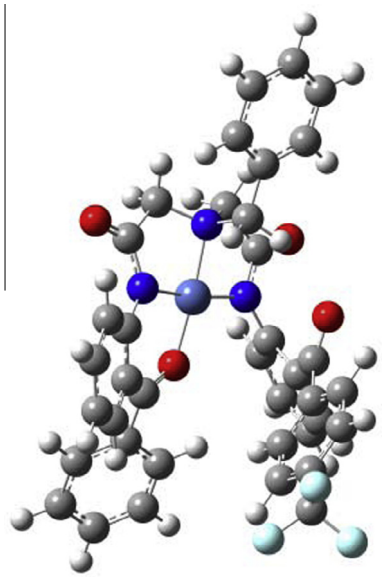

Fig. 9. Complex **6b** with coordination of the unsubstituted ligand arm and with the ligand arm bearing the $-CF_3$ group *cis* to the benzyl group.

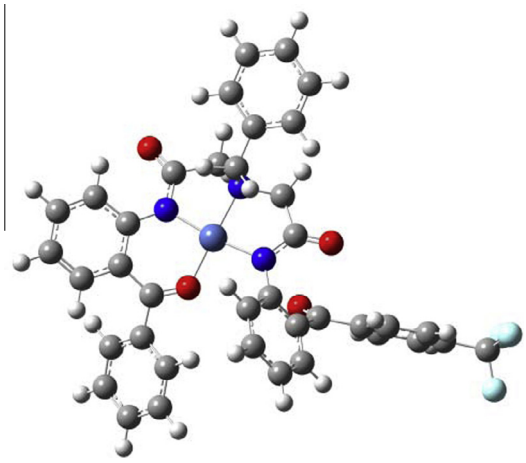

Fig. 10. Complex **6b** with coordination of the unsubstituted ligand arm and with the ligand arm bearing the $-CF_3$ group *trans* to the benzyl group.

ΔG values for the four structural permutations of complexes **6a**–**h** without and upon inclusion of the solvent model.

Overall though, the results with respect to relative energies are heavily dependent upon inclusion of the solvent model considering each complex individually with respect to the dominance of one structure over the other three with respect to coordination site and relative configuration (for example, complex **6f** has three close-in-energy minima structures). It is worth noting that while the relative energies change, the geometrical changes of each structure from the gas phase upon inclusion of the solvent were quite small by inspection, thus pertaining to the important role that the solvent plays in stabilizing the complexes without structural changes.

With respect to the coordination site, with the exception of the methyl-substituted complex **6a**, the expected ligand arm coordination preference for each complex is predicted to be energetically favored, though the pronounced differences in the gas phase could be quite muted when the solvent model was included, e.g. complexes **6b**,**d**,**f**. For the methyl-substituted complex **6a**, the methyl group is a weak electron donor and thus it is not too surprising that

Table 2
DFT-calculated Gibbs' Free Energies (ΔG) of four selected coordination site/relative configuration permutations for complexes **6a**–**h**, both without and upon inclusion of a solvent model for CH_2Cl_2.

	ΔG in the gas phase (kJ mol^{-1})				ΔG with the solvent model for CH_2Cl_2 (kJ mol^{-1})			
Coordination site:	First sidearm listed		Second sidearm listed		First sidearm listed		Second sidearm listed	
Relative configuration:	*trans* (*R**,*R**)	*cis* (*R**,*S**)	*trans* (*R**,*R**)	*cis* (*R**,*S**)	*trans* (*R**,*R**)	*cis* (*R**,*S**)	*trans* (*R**,*R**)	*cis* (*R**,*S**)
6a: –*p*-H, –*o*-Me	0.00	5.10	2.84	7.19	0.00	2.74	1.75	3.74
6b: –*p*-H, –*p*-CF_3	0.00	5.34	4.98	9.05	0.00	3.65	0.79	6.47
6c: –*p*-H, –*p*-CF_3	0.00	4.52	6.18	9.82	0.00	4.76	4.79	7.43
6d: –*p*-H, –*p*-OMe	2.12	5.92	0.00	2.66	0.83	5.76	0.00	3.97
6e: –*p*-OMe, –*p*-CF_3	0.00	13.43	7.92	15.25	0.00	6.40	9.39	13.80
6f: –*p*-H, –*o*-CF_3	0.00	4.44	5.36	12.30	0.00	0.15	0.46	2.54
6g: –*p*-OMe, –*o*-CF_3	0.00	3.65	7.20	10.30	0.00	3.80	2.69	5.85
6h: –*p*-OMe, –*o*-CF_3	0.00	7.13	6.83	11.99	0.00	8.85	1.87	7.52

the expected results were not forthcoming though for complex **6a** the difference is quite small at 1.75 kJ mol^{-1} with inclusion of the solvent model. It is worth noting that steric effects do not appear to play a role in the calculational results as the methyl group is oriented away from any potential steric interactions. These results tally well with the X-ray crystal structure determinations of complexes **6b**,**c**,**f**–**h** wherein the expected coordination configuration was indeed observed for these complexes in the solid state. For complex **6a**, the expected coordination configuration was observed in the solid state in contrast to the calculational result. Interestingly, for complex **6d**, the unexpected coordination configuration observed in the solid state was in opposition to intuition and the calculational results, but it must be noted that for this complex the difference in energies – at least with inclusion of the solvent model – between the two coordination configurations was near the lowest of all the complexes at 0.83 kJ mol^{-1} thereby suggesting that the presence of the unexpected coordination configuration isomer is not altogether untoward. Perhaps even more surprising was the result for complex **6e** where both coordination configuration isomers were observed in the solid state with the expected isomer – in concert with calculations – predominant (ratio adjudged to be ca. 9:1). Here though, the difference in energies between the two coordination configurations was near the highest of all the complexes (9.39 kJ mol^{-1} with the solvent model).

In four cases fine or reasonable agreement was found between prediction and observation for the position of the coordination site equilibrium in solution, viz. complexes **6b**,**c**,**f**,**g**, which is respectable considering the complexity of the systems involved, their conformational mobility and the need to include a solvent model. In the case of complex **6b**, the experimental value of ΔG was evaluated as 0.69 kJ mol^{-1} between the global minimum and the next lowest energy structure with other structures of minimal contribution and this compared well with the calculations which provided a value of 0.79 kJ mol^{-1}; for complex **6f**, the experimental value of ΔG was evaluated as 1.04 kJ mol^{-1} between the preferred coordination configuration isomer and the alternative coordination configuration isomer while calculations provided a value of 0.46 kJ mol^{-1}; for complex **6g**, the observed value of 4.42 kJ mol^{-1} was somewhat higher than the predicted value of 2.69 kJ mol^{-1}; and by contrast, for complex **6c** the observed value of 2.86 kJ mol^{-1} was somewhat lower than the predicted value of 4.79 kJ mol^{-1}. Of note, in the case of complex **6c**, considerable improvement was forthcoming by inclusion of the solvent model (calculated ΔG with respect to coordination in the gas phase, 6.18 kJ mol^{-1}). For complex **6b**, inclusion of the solvent model was absolutely critical for the good result (calculated ΔG with respect to coordination in the gas phase, 4.98 kJ mol^{-1}) and similarly for complexes **6g** (calculated ΔG with respect to coordination in the gas phase, 7.20 kJ mol^{-1}) and **6f** (calculated ΔG with respect to coordination in the gas phase, 5.36 kJ mol^{-1}). In two other cases where the dynamic behavior could be comprehended – complexes **6e** (exp. 2.47 kJ mol^{-1}; calc. 9.39 kJ mol^{-1}) and **6h** (exp. 5.54 kJ mol^{-1}; calc. 1.87 kJ mol^{-1}) – experimental observations were less in concert with calculated values. For these two cases, inclusion of the solvent model actually led to poorer predicted values. The reasons for these anomalies may again reside with the complex conformational behavior of the molecules stemming from their promiscuity with respect to conformational space. Clearly inclusion of a solvent model influences the results greatly and therefore must be considered mandatory for these complexes. Nonetheless, modeling calculations hold promise for predicting favorable selection of systems for coordination configuration and stereochemical preference and hence potential application as optically switchable devices. The challenge is in surmounting the encumbrance arising from the complex behavior of these highly conformationally promiscuous molecules.

3. Conclusions

It was found that control of the stereochemical preference between (*S**,*S**) and (*S**,*R**) diastereomers by substituent modification of the ligand sidearms was possible in the solid state with the preferred coordination of the sidearms generally consistent with expectations based on the electron-donating or -withdrawing properties of the sidearm substituent groups. However, it seems that only for complexes with *ortho* substituents (complexes **6a**,**f**–**g**) are strong preferences for the coordination manner necessarily displayed in the solid state based on the electron-withdrawing or -donating properties of the substituents. In other cases with only *para* substituents present (**6b**–**e**), the observed preference for the coordination manner may align with the expected preference, though this may simply be incidental (**6b**,**c**), or it may provide an unexpected mixture (**6e**), or it may provide a seemingly anomalous result counter to chemical intuition (**6d**). The unusual observation of mixed species in one crystal lattice in the case of **6e** is an interesting crystallographic result and may be the consequence of the state of the system in solution.

These results indicate that the design of molecular systems sensitive to external stimuli with macromolecular structure may be less predictable than originally thought, but this could lead to greater potential in terms of response sensitivity and fine tuning.

4. Experimental

4.1. X-ray experimental

The crystal data and details of data collection are given in Table 1. X-ray diffraction data for complexes **6a**,**c**,**d** were measured

at 123(2) K using synchrotron radiation on the BL40XU (**6c**,**d**) and BL02B2 (**6a**) instruments at SPring-8 utilizing a high precision diffractometer [11] and large cylindrical image-plate camera [12], respectively, because of the extremely small crystal sizes of the samples provided. The data for complexes **6b**,**e** were measured using a Rigaku R-AXIS RAPD imaging plate diffractometer {graphite-monochromated Mo Kα or Cu Kα radiation, ω-scan technique, λ = 0.71073 (**6e**) or 1.54186 (**6b**) Å} at 123(2) (**6e**) or 143(2) (**6b**) K. The crystal structures were solved by direct methods using SHELXS-97 [13] and all non-H atoms were refined on F^2 anisotropically using SHELXL-97 [14] except for **6a**. H atoms were located by geometrical calculations and included refinement using riding models with constrained isotropic displacement parameters. The structure for **6a** was refined isotropically except for the Pd atom due to the very weak diffraction intensities as a result of the small crystal size. However, the molecular structure of **6a** is considered sufficiently reliable and the *R*1 factor converged to 0.0298 without significant residual electron density peak. Depictions of the X-ray derived structures in Figs. 2–6 were produced using the GUI GaussView [15].

4.2. NMR experimental

NMR spectra were acquired using a Bruker Avance NMR spectrometer equipped with a 5 mm normal configuration dual coil probe with z-gradient capability at a field strength of 9.4 T operating at 400 and 376 MHz for ^{1}H and ^{19}F nuclei, respectively. NMR spectra for the intermediates and the free ligands were measured at a field strength of 7.05 T operating at 300 and 75.5 MHz for ^{1}H and ^{13}C nuclei, respectively Measurements were conducted at 25 °C (or at other temperatures as indicated for the complexes **6a**–**e**) with samples contained in $CDCl_3$ (in CD_2Cl_2 for the complexes **6a**–**e**). The chemical shifts of ^{1}H and ^{13}C nuclei are reported relative to TMS incorporated as an internal standard (δ = 0 ppm for both ^{1}H and ^{13}C) and externally to CF_3CO_2H in $CDCl_3$ [2–3%v/v] at 25 °C for ^{19}F (δ = −78.5 ppm). Correction of the recorded temperature was effected by a Pt100 thermocouple inserted into the probe. General NMR experimental details have been previously described [16].

4.3. Molecular modeling experimental

DFT quantum chemical calculations were performed using the Gaussian09 [17] program and analyzed using the GUI GaussView [15]. Depictions of the structures in Figs. 7–10 were produced using the GUI GaussView [15]. The modeling protocol consisted of initial optimization in the gas phase using the restricted B3LYP functional [18] with the 6-31G(d,p) basis set for non-metallic atoms and the LanL2DZ basis set for Ni and Pd whereby for these entities core electrons were substituted by a model potential by invoking the keyword *pseudo* = *read*. Geometry optimizations were conducted in tandem with vibrational analysis and thermochemistry calculations at the same level of theory. Vibrational analyses were conducted to confirm that optimized structures were true minima on the potential energy surface by not providing imaginary frequencies and to obtain the thermodynamic contributions to Δ*G* at 298.15 K and 1 atm wherein frequencies were scaled by a factor of 0.9806 [19]. Each structure for optimization was conveniently modified from an optimized structure taken from a set for a compound previously optimized, this ensured not only computational efficiency but that direct comparisons were valid and meaningful. The first structure of a set to be optimized was taken from an X-ray crystallographic structure as this has proven a useful tactic in past studies [20] with the optimized structure then providing a basis for the set of structures for that first complex by appropriate modification. Re-optimization at the same level of theory of each gas phase-optimized structure with inclusion of a solvent model – the polarizable continuum model using the integral equation formalism variant solvent model (IEFPCM) – followed previous protocol [21] with parameter values for CH_2Cl_2 as the selected solvent.

4.4. Synthesis

4.4.1. General procedure for the syntheses of 2-aminobenzophenones *2*

To a solution of the corresponding acetamide **1a**–**c** in acetone (0.15 m), aqueous 6 m HCl (40 eq.) was added. The solution was stirred at 70 °C for 2 h followed by the addition of K_2CO_3 until basic. The crude amine was extracted with CH_2Cl_2 and the organic layer dried over Na_2SO_4 and then concentrated in vacuo after filtration. The resulting 2-aminobenzophenones **2a**–**c** were used without further purification.

*4.4.1.1. 2-Amino-2′-methylbenzophenone (**2a**).* 97% yield. ^{1}H NMR δ 2.31 (3H, s), 6.44 (2H, br), 6.56 (ddd, *J* = 8.1, 7.6, 1.1 Hz), 6.75 (dd, *J* = 8.3, 0.7 Hz), 7.23–7.41 (6H, m). ^{13}C NMR δ 19.1, 115.1, 116.6, 117.7, 124.9, 126.7, 128.8, 130.2, 134.4, 134.5, 134.6, 140.3, 151.1, 200.9. HRMS: calcd for $C_{14}H_{14}NO$ $[M+H]^+$ 212.1075, found 212.1079.

*4.4.1.2. 2-Amino-4′-(trifluoromethyl)benzophenone (**2b**).* 90% yield. ^{1}H NMR δ 6.25 (2H, brs), 6.64 (ddd, *J* = 8.1, 7.6, 1.1 Hz), 6.79 (dd, *J* = 8.3, 0.6 Hz), 7.33–7.41 (2H, m), 7.76 (4H, s). ^{13}C NMR δ 115.6, 117.2, 123.9 (qt, $^1J_{F,C}$ = 272.6 Hz), 125.2 (qt, $^3J_{F,C}$ = 3.6 Hz), 127.4, 129.1, 132.4 (qt, $^2J_{F,C}$ = 32.5 Hz), 134.4, 134.9, 143.5, 151.4, 197.7. ^{19}F NMR δ −62.8. HRMS: calcd for $C_{14}H_{11}F_3NO$ $[M+H]^+$ 266.0793, found 266.0799.

*4.4.1.3. 2-Amino-4′-(methoxy)benzophenone (**2c**).* 98% yield; data consistent with literature [22].

4.4.2. General procedure for the syntheses of bromoacetamides *3*

To a suspension of the corresponding 2-aminobenzophenone **2a**–**c** and K_2CO_3 (5 eq.) in MeCN (0.3 m), bromoacetyl bromide (2 eq.) was added dropwise. The mixture was stirred at rt for 2 h followed by the addition of H_2O. The crude amide was extracted with CH_2Cl_2 and the organic layer dried over Na_2SO_4 and then concentrated in vacuo after filtration. The resulting bromoacetamides **3a**–**c** were used without further purification.

*4.4.2.1. 2-(Bromoacetamido)-2′-methylbenzophenone (**3a**).* 95% yield. ^{1}H NMR δ 2.34 (3H, s), 4.09 (2H, s), 7.11 (ddd, *J* = 8.1, 7.6, 1.0 Hz), 7.27–7.35 (3H, m), 7.40–7.47 (m), 7.47 (dd, *J* = 8.0, 1.5 Hz), 7.63 (ddd, *J* = 8.8, 7.9, 1.6 Hz), 8.76 (dd, *J* = 8.4, 0.7 Hz), 12.18 (brs). ^{13}C NMR δ 19.7, 29.5, 120.7, 123.0, 123.3, 125.2, 128.9, 130.2, 130.8, 134.3, 134.9, 135.9, 138.8, 140.3, 165.2, 202.3. HRMS: calcd for $C_{16}H_{15}BrNO_2$ $[M+H]^+$ 332.0286, found 332.0286.

*4.4.2.2. 2-(Bromoacetamido)-4′-(trifluoromethyl)benzophenone (**3b**).* 97% yield. ^{1}H NMR δ 4.07 (2H, s), 7.20 (t, *J* = 7.6 Hz), 7.57 (dd, *J* = 7.9, 1.3 Hz), 7.68 (t, *J* = 7.9 Hz), 7.81 (2H, d, *J* = 8.4 Hz), 7.84 (2H, d, *J* = 8.4 Hz), 8.67 (d, *J* = 8.4 Hz), 11.55 (brs). ^{13}C NMR δ 29.4, 121.6, 123.1, 123.2 (qt, $^1J_{F,C}$ = 270.7 Hz), 125.3 (qt, $^3J_{F,C}$ = 3.5 Hz), 129.8, 130.0, 133.5, 133.8 (qt, $^2J_{F,C}$ = 33.1 Hz), 134.8, 139.8, 141.4, 165.0, 198.1. ^{19}F NMR δ −63.0. HRMS: calcd for $C_{16}H_{12}BrF_3NO_2$ $[M+H]^+$ 386.0004, found 386.0007.

*4.4.2.3. 2-(Bromoacetamido)-4′-(methoxy)benzophenone (**3c**).* 88% yield; data consistent with literature [5].

4.4.3. General procedure for the synthesis of ligands *5*

To a solution of the corresponding bromoacetamide **3a**–**c** and benzylamine **4** [7c] (1 eq.) in MeCN (0.3 m), *i*-Pr_2NEt (2 eq.) was

added. The mixture was stirred at 70 °C for 16 h and then concentrated in vacuo. The product was purified by column chromatography over silica (hexane–EtOAc, gradient from 5:1 to 1:1) to provide the resulting ligands **5a**–**c**.

*4.4.3.1. N-(2-Benzoylphenyl)-2-(benzyl(2-((2-(2-methylbenzoyl)phenyl)amino)-2-oxoethyl)amino)acetamide (**5a**).* 85% yield. ^{1}H NMR δ 2.26 (3H, s), 3.47 (2H, s), 3.48 (2H, s), 3.96 (2H, s), 7.08 (ddd, J = 8.2, 7.6, 1.1 Hz), 7.15 (td, J = 7.6, 1.1 Hz), 7.21–7.31 (6H, m), 7.38–7.47 (4H, m), 7.48–7.52 (4H, m), 7.54–7.61 (2H, m), 7.66–7.71 (2H, m), 8.22 (d, J = 8.0 Hz), 8.67 (dd, J = 8.4, 0.8 Hz), 10.89 (brs), 11.95 (brs). ^{13}C NMR δ 19.6, 58.7, 59.0, 59.5, 121.1, 122.6, 123.1, 124.0, 125.1, 127.1, 127.6, 128.0, 128.2, 128.3, 129.5, 129.8, 130.2, 130.8, 131.8, 132.3, 132.7, 133.9, 134.6, 136.3, 137.8, 137.9, 138.8, 140.1, 169.1, 169.5, 197.4, 201.7. HRMS: calcd for $C_{38}H_{34}N_3O_4$ $[M+H]^+$ 596.2549, found 596.2561.

*4.4.3.2. N-(2-Benzoylphenyl)-2-(benzyl(2-oxo-2-((2-(4-(trifluoromethyl)benzoyl)phenyl)amino)ethyl)amino)acetamide (**5b**).* 85% yield. ^{1}H NMR δ 3.39 (2H, s), 3.41 (2H, s), 3.84 (2H, s), 7.13–7.23 (5H, m), 7.41–7.48 (5H, m), 7.50–7.63 (4H, m), 7.65–7.70 (4H, m), 7.79 (2H, d, J = 8.1 Hz), 8.25 (dd, J = 8.3, 0.6 Hz), 8.40 (dd, J = 8.2, 0.5 Hz), 11.01 (brs), 11.15 (brs). ^{13}C NMR δ 59.2, 59.3, 59.7, 122.2, 122.9, 123.3, 123.5 (qt, $^1J_{F,C}$ = 272.7 Hz), 125.1 (qt, $^3J_{F,C}$ = 3.4 Hz), 125.7, 126.4, 127.8, 128.2, 128.4, 129.6, 130.0, 130.1, 131.9, 132.5, 132.6, 133.5, 133.5, 133.6 (qt, $^2J_{F,C}$ = 32.5 Hz), 135.9, 138.0, 138.2, 138.6, 141.0, 169.0, 169.2, 196.5, 198.5. ^{19}F NMR δ −63.0. HRMS: calcd for $C_{38}H_{31}F_3N_3O_4$ $[M+H]^+$ 650.2267, found 650.2270.

*4.4.3.3. N-(2-Benzoylphenyl)-2-(benzyl(2-((2-(4-methoxybenzoyl)phenyl)amino)-2-oxoethyl)amino)acetamide (**5c**).* 84% yield. ^{1}H NMR δ 3.35 (4H, s), 3.79 (2H, s), 3.88 (3H, s), 6.87–6.92 (2H, m), 7.11–7.23 (5H, m), 7.37–7.44 (4H, m), 7.50–7.60 (5H, m), 7.66–7.73 (4H, m), 8.26–8.31 (2H, m), 10.87 (brs), 11.00 (brs). ^{13}C NMR δ 55.4, 59.1, 59.1, 59.5, 113.4, 122.5, 122.6, 123.0, 123.1, 126.8, 127.2, 127.6, 128.0, 128.3, 129.6, 129.9, 130.4, 131.6, 132.2, 132.4, 132.5, 133.0, 136.0, 137.8, 138.0, 138.2, 163.3, 168.9, 169.0, 196.3, 197.8. HRMS: calcd for $C_{38}H_{34}N_3O_5$ $[M+H]^+$ 612.2498, found 612.2513.

*4.4.4. Synthesis of 2-(benzyl(2-((2-(4-methoxybenzoyl)phenyl)amino)-2-oxoethyl)amino)-N-(2-(4-(trifluoromethyl)benzoyl)phenyl)acetamide (**8**)*

To a solution of the bromoacetamide **3c** and benzylamine **7** [5] (1 eq.) in MeCN (0.3 m), *i*-Pr_2NEt (2 eq.) was added. The mixture was stirred at 70 °C for 16 h and then concentrated in vacuo. The product was purified by column chromatography over silica (hexane–EtOAc, gradient from 2:1 to 1:1) to provide **8** in 87% yield. ^{1}H NMR δ 3.37 (2H, s), 3.38 (2H, s), 3.80 (2H, s), 3.90 (3H, s), 6.89–6.94 (2H, m), 7.13–7.25 (5H, m), 7.41–7.61 (6H, m), 7.64–7.72 (4H, m), 7.80 (2H, d, J = 8.1 Hz), 8.24 (d, J = 7.6 Hz), 8.33 (d, J = 7.7 Hz), 10.93 (brs), 10.99 (brs). ^{13}C NMR δ 55.4, 59.1, 59.3, 59.6, 113.5, 122.4, 122.9, 123.0, 123.4, 123.5 (qt, $^1J_{F,C}$ = 272.5 Hz), 125.0 (qt, $^3J_{F,C}$ = 3.4 Hz), 126.6, 126.7, 127.7, 128.4, 129.6, 130.1, 130.3, 131.8, 132.6, 132.7, 133.4, 133.5 (qt, $^2J_{F,C}$ = 32.5 Hz), 135.9, 138.0, 138.1, 141.0, 163.4, 168.8, 169.1, 196.3, 196.7. ^{19}F NMR δ −63.0. HRMS: calcd for $C_{39}H_{33}F_3N_3O_5$ $[M+H]^+$ 680.2372, found 680.2387.

*4.4.5. General procedure for the synthesis of Pd^{II} complexes **6a**,**c***

To a solution of the corresponding ligand **5a**–**b** in MeOH (0.04 m), $PdCl_2$ (2 eq.) and K_2CO_3 (6 eq.) were added. The mixture was stirred at 70 °C for 16 h followed by the addition of H_2O. The crude complex was extracted with CH_2Cl_2 and the organic layer dried over Na_2SO_4 and then concentrated in vacuo after filtration. The product was purified by column chromatography over silica (CH_2Cl_2–acetone, gradient from 2:1 to 1:10) to provide the resulting complexes **6a**,**c**.

*4.4.5.1. Pd^{II} complex **6a**.* 8% yield. Detailed assignment of proton absorptions was not possible due to intense molecular movements HRMS: calcd for $C_{38}H_{32}N_3O_4Pd$ $[M+H]^+$ 700.1428, found 700.1458.

*4.4.5.2. Pd^{II} complex **6c**.* 26% yield. ^{1}H NMR (major isomer, 35 °C) δ 3.44 (2H, vbs), 3.59 (1H, vbs), 3.68 (1H, vbs), 3.82 (2H, vbs), 7.23–7.31 (5H, m), 7.39–7.48 (8H, m), 7.533 (2H, ∼t, J = 7.51 Hz), 7.57–7.62 (1H, m), 7.647 (3H, ∼d_{AB}, J = 8.14 Hz), 7.807 (3H, ∼d_{AB}, J = 7.01 Hz). ^{19}F NMR (35 °C) δ −64.07. HRMS: calcd for $C_{38}H_{29}F_3N_3O_4Pd$ $[M+H]^+$ 754.1145, found 754.1169.

*4.4.6. General procedure for the synthesis of Ni^{II} complexes **6b**,**d**,**e***

To a solution of the corresponding ligand **5b**–**c** or **8** in MeOH (0.1 m), $Ni(NO_3)_2{\cdot}6H_2O$ (2 eq.) and KOH (7 eq.) were added. The mixture was stirred at 70 °C for 7 h followed by the addition of H_2O. The crude complex was extracted with CH_2Cl_2 and the organic layer dried over Na_2SO_4 and then concentrated in vacuo after filtration. The product was purified by column chromatography over silica (CH_2Cl_2–acetone, gradient from 2:1 to 1:10) to provide the resulting complexes **6b**,**d**,**e**.

*4.4.6.1. Ni^{II} complex **6b**.* 52% yield. ^{1}H NMR (35 °C) δ 3.004 (1H, d_{AB}, J = −15.38 Hz), 3.116 (1H, d_{AB}, J = −15.73 Hz), ∼3.37 (1H, vbs), 3.542 (1H, bd_{AB}, J = −15.51 Hz), ∼3.63 (1H, vbs), 3.825 (1H, bd_{AB}, J = −11.07 Hz), 7.055 (1H, ∼t, J = 7.58 Hz), 7.18–7.39 (8H, m), 7.40–7.59 (6H, m), 7.60–7.72 (4H, m), 7.875 (3H, ∼d, J = 7.27 Hz). ^{19}F NMR (35 °C) δ −66.08. HRMS: calcd for $C_{38}H_{29}F_3N_3O_4Ni$ $[M+H]^+$ 706.1464, found 706.1666.

*4.4.6.2. Ni^{II} complex **6d**.* 58% yield. Detailed assignment of proton absorptions was not possible due to intense molecular movements HRMS: calcd for $C_{38}H_{32}N_3O_5Ni$ $[M+H]^+$ 668.1695, found 668.1889.

*4.4.6.3. Ni^{II} complex **6e**.* 41% yield. ^{1}H NMR (35 °C) δ 2.966 (1H, d_{AB}, J = −15.56 Hz), 3.118 (1H, d_{AB}, J = −15.83 Hz), ∼3.26 (1H, vbs), 3.561 (1H, bd_{AB}, J = −15.80 Hz), ∼3.58 (1H, vbs, ol), 3.807 (3H, s), ∼3.84 (1H, vbd, ol), 6.778 (2H, ∼d, J = 8.97 Hz), 7.038 (1H, ∼t, J = 7.54 Hz), 7.11–7.20 (2H, m), 7.22–7.29 (1H, m), 7.30–7.37 (3H, m), 7.38–7.52 (5H, m), 7.654 (2H, ∼d_{AB}, J = 8.28 Hz), 7.72–7.81 (2H, m), 7.82–7.89 (2H, m), 7.913 (1H, ∼d, J = 8.51 Hz). ^{19}F NMR (35 °C) δ −66.02. HRMS: calcd for $C_{39}H_{31}F_3N_3O_5Ni$ $[M+H]^+$ 736.1569, found 736.1759.

Acknowledgments

Guangqian Zhang is thanked for assistance with parts of the experimental work; financial support from the Center for International Mobility (CIMO) and Turun Yliopistosäätiö, Ikerbasque, Basque Foundation for Science, and the Basque Government (SAIOTEK S-PE13UN098) is gratefully acknowledged; the CSC–IT Center for Science Ltd. is thanked for providing computational resources and assistance with modeling calculations (Nino Runeberg); the Japan Synchrotron Radiation Research Institute (JASRI) is thanked for the synchrotron radiation experiments which were performed on the BL02B1 and BL40XU instruments at SPring-8 (Proposal Nos. 2010A1976, 2010B1489, and 2010B1494), and SGIker (UPV/EHU) is thanked for HRMS analyses.

Appendix A. Supplementary material

CCDC 990583 for (**6a**), 990584 for (**6b**), 990585 for (**6c**), 990586 for (**6d**), and 990587 for (**6e**) contains the supplementary

crystallographic data for this paper. These data can be obtained free of charge from The Cambridge Crystallographic Data Centre via www.ccdc.cam.ac.uk/data_request/cif. Supplementary data associated with this article can be found, in the online version, at http://dx.doi.org/10.1016/j.ica.2015.04.029.

References

[1] (a) M. Köberl, M. Cokoja, W.A. Herrmann, F.E. Kühn, Dalton Trans. 40 (2011) 6834;
(b) C.V. Kumar, B. Raju, Mol. Supramol. Photochem. 8 (2001) 505;
(c) F.M. Raymo, F.J. Stoddart, Cur. Opin. Colloid Interface Sci. 3 (1998) 150.
[2] F.M. Raymo, Adv. Mater. 14 (2002) 401.
[3] (a) T. Kawamoto, B.S. Hammes, B. Haggerty, G.P.A. Yap, A.L. Rheingold, A.S. Borovik, J. Am. Chem. Soc. 118 (1996) 285;
(b) A.J. Preston, G. Fraenkel, A. Chow, J.C. Gallucci, J.R. Parquette, J. Org. Chem. 68 (2003) 22;
(c) Y. Hamuro, S.J. Geib, A.D. Hamilton, Angew. Chem., Int. Ed. Engl. 33 (1994) 446.
[4] (a) V.A. Soloshonok, H. Ueki, J.L. Moore, T.K. Ellis, J. Am. Chem. Soc. 129 (2007) 3512;
(b) V.A. Soloshonok, H. Ueki, Synthesis (2010) 49;
(c) V.A. Soloshonok, J.L. Aceña, H. Ueki, J. Han, Beilstein J. Org. Chem. 8 (2012) 1920.
[5] J. Han, T. Ono, H. Uekusa, K.D. Klika, V.A. Soloshonok, Dalton Trans. 43 (2014) 5375.
[6] W. Lu, G. Du, K. Liu, L. Jiang, J. Ling, Z. Shen, J. Phys. Chem. A 118 (2014) 283.
[7] (a) V.A. Soloshonok, H. Ueki, T.K. Ellis, Tetrahedron Lett. 56 (2005) 941;
(b) V.A. Soloshonok, H. Ueki, T.K. Ellis, T. Yamada, Y. Ohfune, Tetrahedron Lett. 46 (2005) 1107;
(c) T.K. Ellis, H. Ueki, T. Yamada, Y. Ohfune, V.A. Soloshonok, J. Org. Chem. 71 (2006) 8572;
(d) V.A. Soloshonok, H. Ueki, T.K. Ellis, Synlett (2009) 704.
[8] (a) J.L. Moore, S.M. Taylor, V.A. Soloshonok, ARKIVOC (2005) 287;
(b) V.A. Soloshonok, T.K. Ellis, H. Ueki, T. Ono, J. Am. Chem. Soc. 131 (2009) 7208;
(c) A.E. Sorochinsky, H. Ueki, J.L. Aceña, T.K. Ellis, H. Moriwaki, T. Sato, V.A. Soloshonok, Org. Biomol. Chem. 11 (2013) 4503;
(d) A.E. Sorochinsky, H. Ueki, J.L. Aceña, T.K. Ellis, H. Moriwaki, T. Sato, V.A. Soloshonok, J. Fluorine Chem. 152 (2013) 114.
[9] H. Ueki, T.K. Ellis, C.H. Martin, V.A. Soloshonok, Eur. J. Org. Chem. (2003) 1954.
[10] T. Gelbrich, T.L. Threlfall, M.B. Hursthouse, CrystEngComm 14 (2012) 5454.
[11] N. Yasuda, H. Murayama, Y. Fukuyama, J. Kim, S. Kimura, K. Toriumi, Y. Tanaka, Y. Moritomo, Y. Kuroiwa, K. Kato, H. Tanaka, M. Takata, J. Synchrotron Rad. 16 (2009) 352.
[12] K. Sugimoto, H. Ohsumi, S. Aoyagi, E. Nishibori, C. Moriyoshi, Y. Kuroiwa, H. Sawa, M. Takata, A.I.P. Conf. Proc. 1234 (2010) 887.
[13] G.M. Sheldrick, SHELXS-97 Program for the Solution of Crystal Structures, Universität Göttingen, 1990.
[14] G.M. Sheldrick, SHELXL-97 Program for the Refinement of Crystal Structures, Universität Göttingen, 1997.
[15] R. Dennington, T. Keith, J. Millam, GaussView, Revision 4.1.2, Semichem Inc., Shawnee Mission, KS, 2009.
[16] (a) J. Mäki, P. Tähtinen, L. Kronberg, K.D. Klika, J. Phys. Org. Chem. 18 (2005) 240;
(b) P. Virta, A. Koch, M.U. Roslund, P. Mattjus, E. Kleinpeter, L. Kronberg, R. Sjöholm, K.D. Klika, Org. Biomol. Chem. 3 (2005) 2924;
(c) V. Nieminen, D.Y. Murzin, K.D. Klika, Org. Biomol. Chem. 7 (2009) 537;
(d) K.D. Klika, J. Bernát, J. Imrich, I. Chomča, R. Sillanpää, K. Pihlaja, J. Org. Chem. 66 (2001) 4416;
(e) E. Balentová, J. Imrich, J. Bernát, L. Suchá, M. Vilková, N. Prónayová, P. Kristian, K. Pihlaja, K.D. Klika, J. Heterocycl. Chem. 43 (2006) 645.
[17] M.J. Frisch, G.W. Trucks, H.B. Schlegel, G.E. Scuseria, M.A. Robb, J.R. Cheeseman, G. Scalmani, V. Barone, B. Mennucci, G.A. Petersson, H. Nakatsuji, M. Caricato, X. Li, H.P. Hratchian, A.F. Izmaylov, J. Bloino, G. Zheng, J.L. Sonnenberg, M. Hada, M. Ehara, K. Toyota, R. Fukuda, J. Hasegawa, M. Ishida, T. Nakajima, Y. Honda, O. Kitao, H. Nakai, T. Vreven, J.A. Montgomery Jr., J.E. Peralta, F. Ogliaro, M. Bearpark, J.J. Heyd, E. Brothers, K.N. Kudin, V.N. Staroverov, R. Kobayashi, J. Normand, K. Raghavachari, A. Rendell, J.C. Burant, S.S. Iyengar, J. Tomasi, M. Cossi, N. Rega, J.M. Millam, M. Klene, J.E. Knox, J.B. Cross, V. Bakken, C. Adamo, J. Jaramillo, R. Gomperts, R.E. Stratmann, O. Yazyev, A.J. Austin, R. Cammi, C. Pomelli, J.W. Ochterski, R.L. Martin, K. Morokuma, V.G. Zakrzewski, G.A. Voth, P. Salvador, J.J. Dannenberg, S. Dapprich, A.D. Daniels, O. Farkas, J.B. Foresman, J.V. Ortiz, J. Cioslowski, D.J. Fox, GAUSSIAN 09, Revision A.01, Gaussian Inc, Wallingford, CT, 2009.
[18] (a) A.D. Becke, Phys. Rev. A 38 (1988) 3098;
(b) C. Lee, W. Yang, R.G. Parr, Phys. Rev. B 37 (1988) 785;
(c) A.D. Becke, J. Chem. Phys. 98 (1993) 5648.
[19] A.P. Scott, L. Radom, J. Phys. Chem. 100 (1996) 16502.
[20] M.U. Roslund, K.D. Klika, R.L. Lehtilä, P. Tähtinen, R. Sillanpää, R.P. Leino, J. Org. Chem. 69 (2004) 18.
[21] (a) P. Tähtinen, A. Bagno, K.D. Klika, K. Pihlaja, J. Am. Chem. Soc. 125 (2003) 4609;
(b) K.D. Klika, M. Budovská, P. Kutschy, J. Fluorine Chem. 131 (2010) 467;
(c) K.D. Klika, M. Budovská, P. Kutschy, Tetrahedron: Asymmetry 21 (2010) 647.
[22] X. Li, X. Huo, J. Li, X. She, X. Pan, Chin. J. Chem. 27 (2009) 1379.